Nigerian Research Journal of Chemical Sciences (ISSN: 2682-6054)
Volume 15, Issue 2, 2026

Passivated Silicon Quantum Dots for Selective Non-Enzymatic Glucose Sensing in Complex Food Matrices

*Hassan Grema, B. U. A. Mustapha, M. Z. Kyari and Ali G. Mohammed
Department of Science Laboratory Technology,
Ramat Polytechnic, Maiduguri, Borno State, Nigeria.
*Corresponding Author: hassangrema4444@gmail.com

Accepted: *October 24, 2026* **Published Online***: November 3, 2026*

ABSTRACT

Traditional enzymatic glucose platforms are limited by high production costs and poor stability under environmental fluctuations. To overcome these issues, this study presents a simple, cost-effective, and environmentally benign one-step hydrothermal approach to synthesize water-soluble, amine-functionalized silicon quantum dots (SiQDs) using aminopropyltriethoxysilane (APTES) and sodium citrate. The resulting EDA-capped SiQDs exhibited strong blue fluorescence under UV light, with an excitation peak at 310 nm and a maximum emission at 440 nm. Characterization via FTIR, HRTEM, and XRD confirmed successful surface passivation with hydroxyl and siloxane groups, a spherical morphology (7–10.5 nm), and a predominantly amorphous structure. Analytical conditions were optimized at a SiQD concentration of 0.5 mg/mL, a pH of 7.4, and an incubation time of 15 min. The non-enzymatic sensor demonstrated a concentration-dependent fluorescence quenching response to glucose via a static or dynamic mechanism. A strong linear relationship was established across 0.5–4.0 mM (R^2 = 0.9902), featuring a limit of detection (LOD) of 0.2 mM and satisfactory reproducibility (RSD = 3.14%). Tested coexisting interferents remained within 100 ± 5% of baseline intensity, and application to mango juice achieved high recoveries (107.5%–114.0%), establishing this platform as a stable, robust alternative for food quality monitoring.

Keywords: Fluorescence quenching, glucose determination, non-enzymatic sensing, silicon quantum dots

INTRODUCTION

Fluorescence spectroscopy plays a vital role in food analysis due to its high sensitivity and selectivity when evaluating complex sample matrices. While the technique has traditionally been limited to inherently luminescent samples, the successful derivatization of non-fluorescent

analytes has significantly expanded its analytical scope. Among these analytes, accurate glucose quantification is highly critical. Beyond clinical diagnostics where it underpins the management of metabolic disorders reliable glucose measurement is equally essential in food production and pharmaceutical manufacturing to monitor fermentation, quality, and product consistency [1,2].

Traditionally, glucose detection relies on enzyme-based sensing platforms, most commonly employing glucose oxidase. While these enzymatic systems deliver reasonable sensitivity, they present severe practical limitations [3]. They frequently exhibit poor long-term operational and storage stability, incur substantial production costs, and are highly sensitive to environmental fluctuations in pH and temperature [3]. Furthermore, their fabrication requires intricate enzyme-immobilization procedures that compromise scalability and reproducibility, causing their performance to degrade considerably in complex, non-physiological environments [3].

To overcome these limitations, non-enzymatic, fluorescence-based sensing approaches have gained attention as stable, simple, and highly sensitive alternatives [4]. Among the various fluorescent nanomaterials investigated, silicon quantum dots stand out due to their robust photostability, adjustable optical behavior, low biological toxicity, and eco-friendly synthesis [5]. However, key challenges remain for routine analytical adoption: SiQD-based sensors often struggle to distinguish glucose from structurally similar coexisting substances, exhibit reduced sensitivity at ultra-low glucose concentrations, and show variable performance when applied to complex real-world matrices [4].

As a result, there is an urgent need to develop a dependable, highly specific, and interference-tolerant non-enzymatic fluorescent glucose biosensor built on silicon quantum dots, one that is particularly well-suited for complex fruit juice. Overcoming these challenges is essential to enable precise, sensitive, and reproducible glucose detection across the biomedical, food, and plant research fields.

Silicon quantum dots represent one class of QDs that has garnered considerable attention owing to their favourable optical characteristics and minimal toxicity. These nanoscale crystalline silicon particles display exceptional photoluminescence quantum yield, prolonged emission lifetimes, and tunable emission wavelengths. Although bulk silicon is an indirect band gap semiconductor with poor light-emission efficiency, quantum confinement effects induce quasi-direct band gap behaviour when particle dimensions are reduced below roughly 5 nm—the

size corresponding to the excitonic Bohr radius. This size-dependent transition, which yields substantially enhanced photoluminescence efficiency with reported quantum yields exceeding 90%, renders SiQDs especially suitable for sensing and bio analytical applications [6, 7].

For SiQD-based enzyme-free glucose sensors, the specific nature of the glucose–SiQD interaction dictates overall analytical performance. Several transduction mechanisms including static and dynamic quenching, Förster resonance energy transfer (FRET), photo-induced electron transfer (PET), and the inner filter effect (IFE) convert molecular recognition events on SiQD surfaces into quantifiable optical signals to boost sensitivity and selectivity [8]. Among these, fluorescence quenching remains the most common strategy. It operates either dynamically via collisional encounters or statically through ground-state complex formation, where glucose binding perturbs the local electronic environment of surface-functionalized SiQDs to scale fluorescence suppression with glucose concentration [9]. Although initially developed for biomedical or food-related purposes, these non-enzymatic fluorescence sensors translate readily to plant matrices, such as extracted sap and tissue homogenates. In this context, fluorescence-based approaches offer distinct benefits, including low detection limits, minimal sample consumption, and rapid turnaround times essential for high-throughput plant phenotyping [10]. However, a principal obstacle in plant applications is intrinsic auto fluorescence from endogenous fluorophores like chlorophyll and carotenoids [11]. To ensure specificity, modern sensor configurations deploy ratiometric detection or select operating wavelengths outside dominant auto fluorescence bands. When combined with targeted sample pretreatments (such as filtration or dilution) and spectral correction strategies, these probes deliver reliable, adaptable glucose quantification in plant extracts and plant-derived foods [11].

MATERIALS AND METHODS

Reagents

3-Aminopropyltriethoxysilane (99%), sodium citrate tribasic dihydrate (≥99.0%), ethylenediamine (EDA90%) and sodium hydroxide were purchased from Sigma–Aldrich (USA), and deionized water was used for the preparation of phosphate buffer (0.1 M). The pH of the buffer solution (pH 7.2) was adjusted using sodium hydroxide (0.1 M). Aqueous solutions were prepared by deionized water (18.2 MΩ. cm, Simplicity, Milli–Q Millipore water purification system). All the reagents were of analytical grade and used without further purification.

Synthesis of Silicon Quantum Dots

Water-soluble fluorescent silicon quantum dots were synthesized via a one-pot hydrothermal method. Briefly, 1.5 g of trisodium citrate dihydrate was dissolved in 25 mL of nitrogen-purged deionized water. Ethylenediamine (250 µL) and APTES (8 mL) were subsequently added, and the mixture was magnetically stirred for 10 min under light-protected conditions to ensure complete homogenization. The resulting precursor solution was transferred into a stainless-steel autoclave and heated at 180 °C for 7 h. After naturally cooling to room temperature, the resulting solution was dialyzed against ultrapure water for 48 h using dialysis tubing to remove unreacted precursors and low-molecular-weight by-products. The purified SiQDs solution was subsequently dried at 40 °C and stored at 4 °C until further use [12].

Characterization of SiQDs

The optical properties of the synthesized SiQDs were characterized at room temperature using a UV–visible spectrophotometer (Thermo Scientific™ Multiskan™ GO) over the wavelength range of 200–800 nm. Fluorescence emission spectra were acquired using a Tecan microplate reader equipped with black 96-well microplates, with instrument operation and data acquisition performed using SPARKCONTROL Magellan software.

The surface functional groups of the SiQDs were identified by Fourier transform infrared spectroscopy (FT-IR) using a Bruker ATR FTIR Alpha spectrometer. The morphology and elemental composition of the synthesized SiQDs were examined by high-resolution transmission electron microscopy coupled with energy-dispersive X-ray spectroscopy (HRTEM-EDX) using a JEOL JEM-2100F microscope. X-ray diffraction (XRD) analysis was subsequently conducted using a Shimadzu XRD-6000 diffractometer equipped with Cu–Kα radiation to determine the structural characteristics and crystallinity of the synthesized SiQDs.

Determination of Silicon Quantum Dots Concentration

To establish the optimum SiQDs concentration for subsequent analysis, solutions with concentrations of 0.5, 1.0, 1.5, and 2.0 mg/mL were prepared and evaluated.

Optimization Parameters

Phosphate buffer solutions within the pH range of 7.0–8.0 were investigated to determine the optimum pH for glucose detection. For each measurement, 200 µL of the buffer solution was

transferred into a black 96-well microplate, followed by the addition of 50 µL of SiQDs suspension and 50 µL of glucose solution (1 mM). The mixture was incubated at room temperature for 10 min, after which the fluorescence response was measured using a microplate reader at excitation and emission wavelengths of 310 and 440 nm, respectively.

Optimization of Reaction Time for SiQD Glucose Interaction

The optimum interaction time between the SiQDs (0.5 mg/mL) and glucose was determined using a freshly prepared glucose solution (1 mM) in 0.1 M phosphate buffer (pH 7.4). The experiment was conducted following the procedure described above, and fluorescence measurements were recorded at 0, 5, 10, 15, 20, 25, 30, 35, and 40 min. The fluorescence response was monitored using a microplate reader at excitation and emission wavelengths of 310 and 440 nm, respectively.

Evaluation of Glucose Concentration Range and Sensor Sensitivity

The analytical performance of the proposed sensing platform was evaluated using glucose concentrations ranging from 0.5 to 5.0 mM. For the control, 50 µL of SiQDs (0.5 mg/mL) was mixed with 250 µL of phosphate buffer solution (pH 7.4) in a black 96-well microplate. For glucose detection, five separate wells were prepared by adding 200 µL of phosphate buffer, 50 µL of glucose solution at the required concentration, and 50 µL of SiQDs (0.5 mg/mL), followed by thorough mixing. The resulting mixtures were incubated at room temperature for 10 min before fluorescence measurement. Fluorescence signals were recorded using a microplate reader at excitation and emission wavelengths of 310 and 440 nm, respectively.

Real Sample Analysis

A commercially available mango juice sample was centrifuged at 10,000 rpm for 10 min prior to glucose determination. The resulting supernatant was diluted 100-fold by mixing 0.1 mL of the juice with 9.9 mL of deionized (DI) water. The diluted sample was then spiked with glucose solutions at concentrations of 4 and 6 mM. Fluorescence measurements were performed using a microplate reader at excitation and emission wavelengths of 310 and 440 nm, respectively. All measurements were conducted in triplicate (n = 3).

Interference Studies

Potential interference from common endogenous ions and compounds, including urea, ascorbic acid, creatinine, sodium chloride, and potassium chloride, was evaluated. Each interfering

species was prepared at a concentration of 0.5 mM and introduced into a sensing mixture containing SiQDs (0.5 mg/mL), glucose (1 mM), and phosphate buffer (pH 7.4). The effect of each potential interference on the fluorescence response toward glucose was examined to assess the selectivity and analytical reliability of the proposed sensing platform.

Reproducibility Study

Five distinct assays were used to examine the synthesised SiQDs to test the sensor's reproducibility (n = 5). The fluorescence intensity of the SiQDs was measured after they were subjected to 1 mM glucose. We computed the average, relative standard deviation (RSD), and standard deviation (SD).

RESULTS AND DISCUSSION

In the present study, silicon quantum dots were synthesized using a simple, cost-effective, and environmentally benign one-step hydrothermal approach. Aminopropyltriethoxysilane and sodium citrate were employed as the silicon precursor and reducing agent, respectively. Under hydrothermal conditions, the siloxane species were reduced by trisodium citrate, thereby forming silicon nuclei. In contrast to previously reported approaches based on bulk silicon or SiO_2 [12, 13], the proposed method eliminates the need for post-synthetic hydrophilic modification of initially hydrophobic SiQDs. The water-soluble nature of APTES also facilitates aqueous dispersion and photostability, while enabling effective interaction with trisodium citrate during the synthesis. As shown in Fig. 1, EDA-capped SiQDs exhibited a substantially enhanced fluorescence intensity compared with the corresponding uncapped SiQDs.

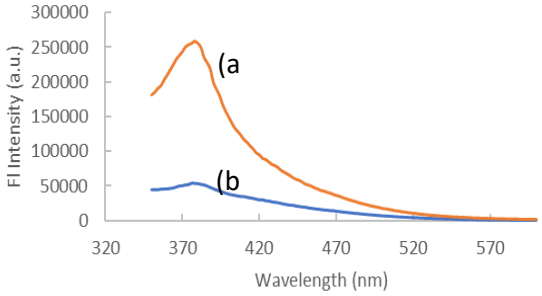


Figure 1: Emission spectra of SiQDs-EDA (a) and SiQDs (b)

UV/Vis and Fluorescence Emission Spectrum of Silicon Quantum Dots

The optical properties of the synthesized SiQDs were investigated by UV–visible absorption and fluorescence spectroscopy. As shown in Fig. 2, the as-prepared SiQDs colloidal solution exhibited a light-yellow translucent appearance under ambient light and produced a distinct blue fluorescence upon irradiation with a portable UV lamp (Fig. 2, inset). A similar blue fluorescence emission from SiQDs under UV irradiation has been previously reported [14].

The UV–visible absorption spectrum of the SiQDs is presented in Fig. 2a. A broad absorption profile was observed across the 200–400 nm region, with a prominent absorption maximum at approximately 329 nm. The observed absorption features are consistent with the characteristic ultraviolet absorption behavior of SiQDs. Previous studies have reported two characteristic absorption bands around 250 and 350 nm, which have been assigned to π–π* and n–π* electronic transitions, respectively [15]. The π–π* transition involves excitation of electrons from π-bonding orbitals to π* antibonding orbitals, whereas the n–π* transition corresponds to excitation of non-bonding electrons to π* orbitals. In addition, Eda et al [12] reported characteristic UV–visible absorption maxima at approximately 280 and 350 nm for SiQDs, further supporting the observed optical characteristics.

The fluorescence emission spectrum of the synthesized SiQDs is shown in Fig. 2b. A maximum emission intensity was observed at 440 nm upon excitation at 310 nm. Accordingly, 310 nm was selected as the optimum excitation wavelength for subsequent fluorescence-based sensing experiments, consistent with the findings reported by Liu et al [16].

.

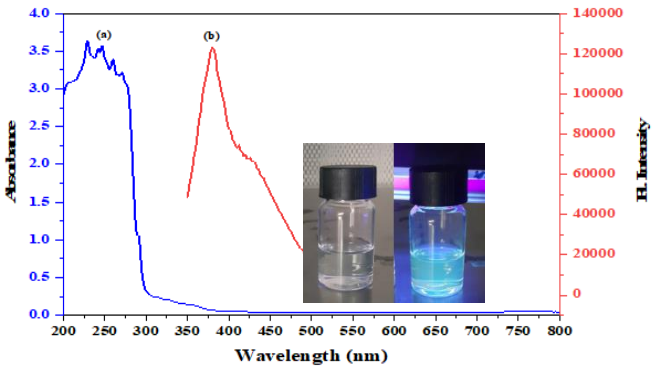


Figure 2: UV/Vis spectrum of SiQDs (a), fluorescence emission of SiQDs (b)

FTIR Analysis of Silicon Quantum Dots

The surface chemistry and functionalization of the synthesized SiQDs were evaluated using Fourier transform infrared (FTIR) spectroscopy (Fig. 3). The spectrum exhibited characteristic absorption bands at 3455, 2914, 1569, 1303, 1112, and 1015 cm^{-1}, confirming successful surface functionalization and partial surface oxidation. Specifically, the broad band at 3455 cm^{-1} is attributed to O–H stretching vibrations from surface hydroxyl groups or adsorbed moisture, which impart hydrophilic character to the SiQDs [17]. Additionally, the peak at 2914 cm^{-1} corresponds to aliphatic C–H stretching vibrations from the synthesis precursors, indicating organic surface passivation [18].

The absorption feature at 1569 cm^{-1} corresponds to C=O stretching vibrations from carbonyl or carboxylate groups, indicating partial surface oxidation [19], which is further supported by the C–O stretching band at 1303 cm^{-1} [20]. Additionally, the intense peaks at 1112 and 1015 cm^{-1} are assigned to Si–O–Si stretching vibrations, confirming the formation of a siloxane framework or a thin silicon oxide surface layer. This oxidation behavior is common in solution-processed SiQDs and typically enhances chemical stability and biocompatibility [17, 21]. Collectively, these FTIR results confirm that the SiQD surfaces are effectively passivated with hydroxyl, aliphatic C–H, carbonyl, C–O, and Si–O–Si functionalities, ensuring excellent aqueous stability for sensing and optoelectronic applications.

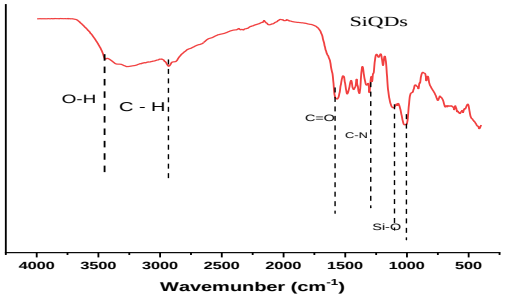


Figure 3. FTIR spectrum of SiQDs

The morphology and particle-size distribution of the synthesized SiQDs were investigated using high-resolution transmission electron microscopy (HRTEM). As shown in Fig. 4, the SiQDs exhibited a predominantly spherical morphology with good dispersion and a relatively uniform particle-size distribution. The particles had diameters ranging from approximately 7 to 10.5 nm. These observations are consistent with previous reports describing SiQDs with spherical morphology and relatively narrow size distributions.

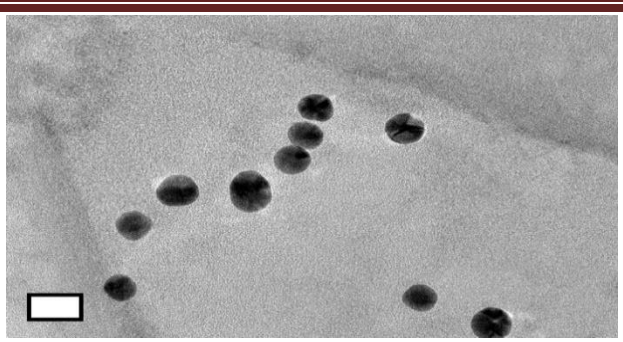


Figure 4: HRTEM pictures of SiQDs at a 200 nm scale.

XRD Analysis of SiQDs

X-ray diffraction (XRD) was employed to evaluate the crystallinity and atomic arrangement of the synthesized SiQDs (Fig. 5) [22]. The XRD pattern exhibited a single broad diffraction peak centered at $2\theta = 21.05°$, confirming a predominantly amorphous structure with short-range atomic ordering characteristic of amorphous silicon, rather than the sharp reflections typical of crystalline silicon [23]. This lack of long-range structural order is further supported by the absence of distinct reflections for crystalline planes like {220} and {311}. The pronounced peak broadening is likely driven by the nanoscale dimensions (<3 nm) of the SiQDs, where quantum confinement and a high density of surface states hinder ordered lattice development [24], alongside low synthesis temperatures and surface-capping species restricting crystal growth. Ultimately, this amorphous structure and short-range ordering directly influence the optical and electronic properties of the SiQDs by modifying their electronic band structure via quantum confinement [25].

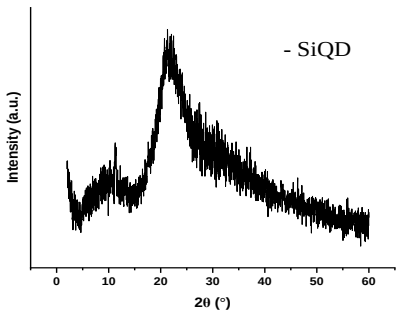


Figure 5: X-ray pattern of the prepared SiQD

Optimization of SiQDs Concentration

The concentration of SiQDs was optimized to obtain the highest fluorescence response for subsequent sensing experiments. Among the concentrations evaluated, 0.5 mg/mL produced the highest fluorescence intensity and was therefore selected as the optimum concentration (Fig. 6). The SiQDs concentration plays a critical role in sensing performance by influencing the availability of surface-active sites, analyte accessibility, and the intensity of the optical response. An appropriate concentration provides sufficient interaction sites for analyte binding while maintaining a favorable signal-to-noise ratio. In contrast, excessively low SiQDs concentrations may result in weak fluorescence signals, whereas higher concentrations can promote particle aggregation, self-quenching, and reduced analyte accessibility [26, 27].

At 0.5 mg/mL, the SiQDs exhibited favorable dispersion, enabling effective interaction with the target analyte while minimizing aggregation-induced fluorescence quenching. The optimized concentration also reduced excessive self-absorption of emitted radiation and provided adequate surface sites for analyte interaction, resulting in the maximum fluorescence response. Therefore, 0.5 mg/mL was selected as the working SiQDs concentration for subsequent analytical measurements.

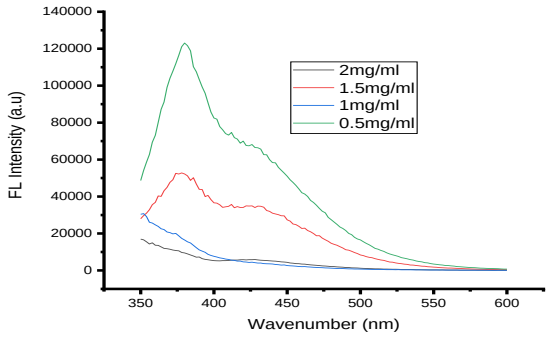


Figure 6: Fluorescence spectra of SiQDs at different concentrations

Optimization of pH and Reaction Time

The effect of pH on the SiQD fluorescence response toward glucose was evaluated using phosphate buffers across a pH range of 7.0–8.0 (Fig. 7a). The fluorescence intensity peaked at pH 7.4, with lower or higher pH values resulting in decreased intensity. The enhanced response at pH 7.4 is attributed to a favorable surface group protonation state that promotes effective

passivation, suppresses non-radioactive recombination [28], and optimizes glucose–SiQD surface interactions [29]. Conversely, higher pH levels cause surface deprotonating, altering charge distribution and inducing alkaline-driven surface oxidation. Because near-neutral conditions (pH 7.0–7.4) consistently maximize stability and analytical performance for fluorescence sensing [29, 30], a pH of 7.4 was selected for subsequent experiments. The incubation time was similarly optimized to establish the reaction kinetics (Fig. 7b).

The fluorescence intensity rose rapidly, peaking at 15 min before gradually declining with prolonged incubation. The initial surge indicates rapid glucose binding to active SiQD surface sites, while the subsequent decline is likely driven by saturation-induced electronic changes or partial nanoparticle aggregation that reduces the effective concentration of dispersed quantum dots [31]. Consequently, an incubation time of 15 min was selected as the optimum reaction period.

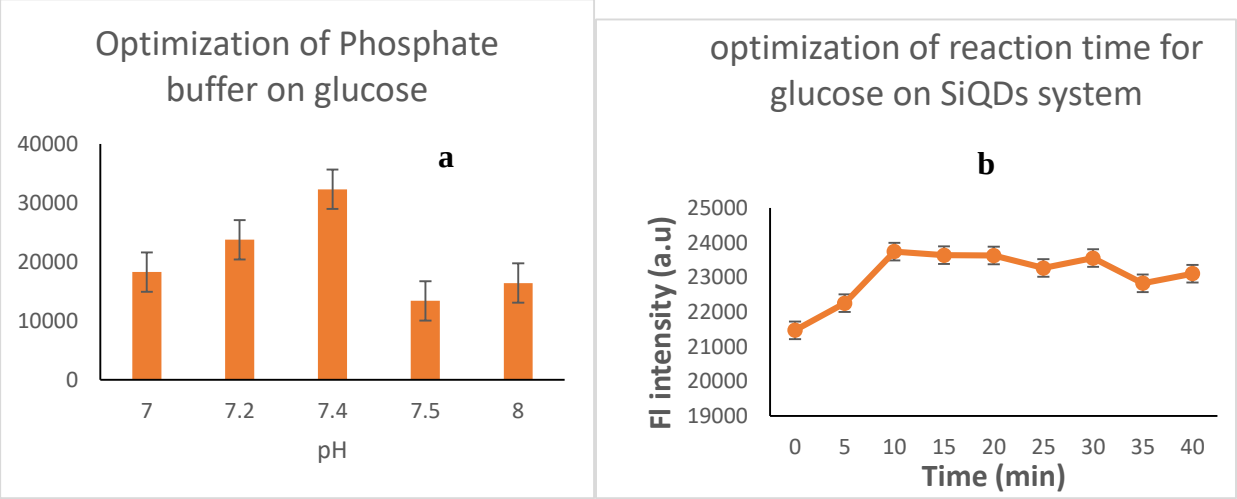


Figure 7: (a) Effect of different pH buffers, (b) reaction time. Experimental condition: 0.5 mg/ml of SiQDs and 0.3 mM of glucose.

Analytical Performance and Calibration

To evaluate the sensitivity of the proposed non-enzymatic assay, various concentrations of glucose were introduced into the colloidal NH_2@SiQD system. As shown in the fluorescence spectra (Figure 8a), the fluorescence intensity exhibited a concentration-dependent attenuation. This quenching mechanism is driven by surface-mediated interactions, where glucose molecules bind to the NH_2@SiQDs via hydrogen bonding and hydrophobic interactions (Figure 8c) [22]. This surface adsorption induces self-aggregation and brings the glucose molecules into close

proximity with the emissive sites. This close proximity facilitates non-radioactive electron or energy transfer, thereby suppressing fluorescence emission [3]. Quantitatively, the sensor exhibited a strong linear relationship over a glucose concentration range of 0.5–4.0 mM (Figure 8b), defined by the regression equation y = 4059x - 1462.9 and a correlation coefficient of R^2 = 0.9902. The limit of detection (LOD) and limit of quantification (LOQ) were calculated to be 0.2 mM and 0.4 mM, respectively. While this LOD is higher than some nanomaterial-based alternatives, the total working range (0–5 mM) and linear range (0.5–4.0 mM) are highly suited for complex food and beverage matrices—such as mango juice—where glucose typically occurs at millimolar levels. Furthermore, triplicate measurements yielded satisfactory reproducibility, confirming high measurement stability. Ultimately, these features highlight the notable advantages of NH_2@SiQDs—including high sensitivity, simplicity, rapid analysis, and cost-effectiveness—validating their practical potential for routine quantitative glucose analysis in commercial mango juice products.

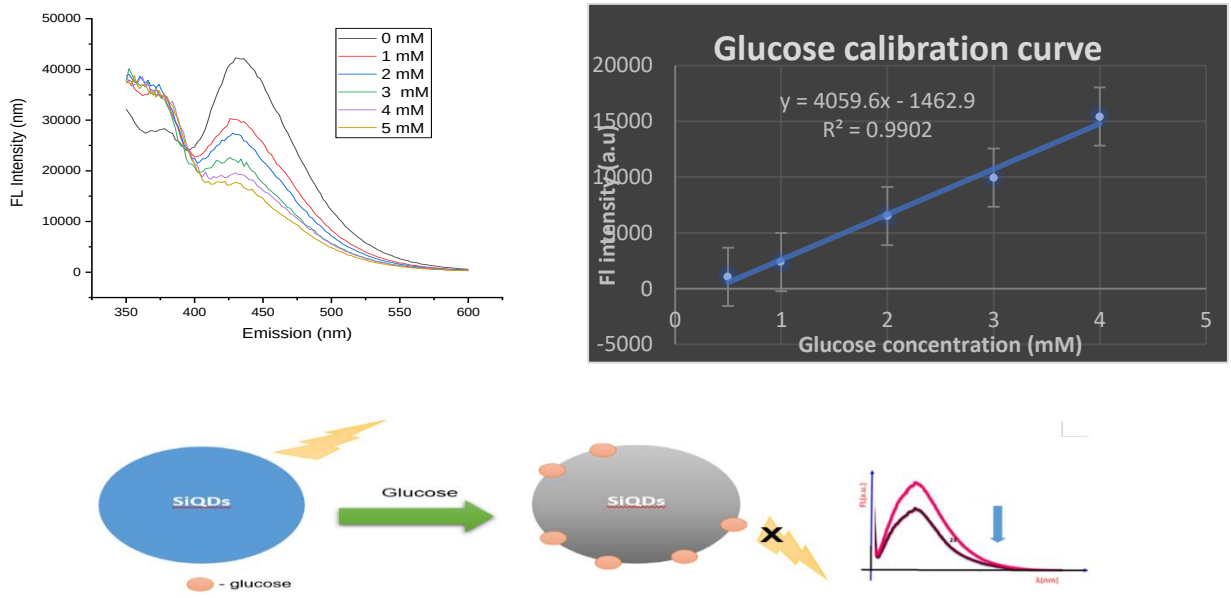


Figure 8: (a) Fluorescence emission spectra of SiQDs (0.5 mg/mL) in phosphate buffer upon exposure to increasing glucose concentrations (0.0–5.0 mM); (b) corresponding calibration curve for glucose over the range 0.0–4.0 mM in PBS (pH 7.4), (c) Schematic illustration of the NH_2@SiQDs for glucose detection

Recovery

The glucose recovery from mango juice, achieved with 0.5 mg/mL silicon quantum dots dispersed in phosphate buffer, is detailed in Table 1. According to the calibration curve (Figure 9), the native glucose level in the juice sample was determined to be 3.4 mM. Recovery percentages for the 4 mM and 6 mM spiked samples varied between 107.50% and 114.00%, underscoring the sensor's efficacy for glucose detection in juice matrices.

Table 1: The recovery of spiked glucose concentrations in mango juice (n= 5)

Sample	Added (mM)	Found (mM)	% Recovery	% Error
Glucose	0.00 4 6	ND 0.43 0.65	ND 107.50 114.00	ND 7.5 13..3

NOTE: ND - not detected

Interference

To evaluate the biosensor's selectivity for real-world applications, the impact of common coexisting interfering species was examined by recording changes in fluorescence intensity at an emission wavelength of 440 nm. While compounds ranging from creatinine to ascorbic acid—alongside urea and Na^+ produced minor negative interference (Table 2 and Fig. 8), the total fluorescence intensity alterations induced by all tested interferents remained strictly within 100 ± 5%. These results confirm the robust selectivity and reliability of the proposed sensor for target glucose detection in complex matrices.

Table 2: Assessment of potential interference in food sample (n=3)

Interfering substance	Concentration (mM)	Change of fluorescence intensity (%)
Creatinine	0.5	-1.8
KCl	0.5	-3.2
Ascorbic acid	0.5	-2.9
Urea	0.5	1.4
NaCl	0.5	2.7

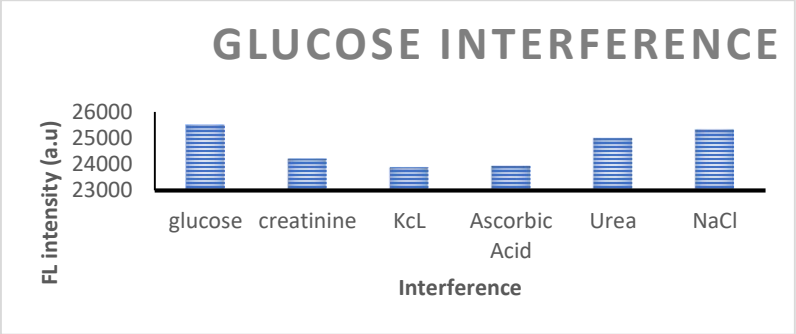


Figure 9: Influence of interference species for glucose determination using the SiQDs system

Reproducibility

The reproducibility of the prepared silicon quantum dots was tested against 0.1 mM of glucose using five different preparations. The relative standard deviation (RSD) obtained was 3.14% (n = 3) for the prepared silicon quantum dots, which indicates good reproducibility of the sensor preparation.

CONCLUSION

Water-soluble, amine-functionalized silicon quantum dots were successfully synthesized via a simple, cost-effective, and environmentally benign one-step hydrothermal approach using APTES and sodium citrate. Structural and optical characterizations confirmed successful surface passivation, a spherical morphology (2–4 nm), and a maximum blue fluorescence emission at 440 nm. Optimized at a concentration of 0.5 mg/mL and a pH of 7.4, the non-enzymatic sensing platform demonstrated a reliable, concentration-dependent fluorescence quenching response to glucose with a linear range of 0.5–4.0 mM, a limit of detection (LOD) of 0.2 mM, and acceptable baseline reproducibility (RSD = 3.14%).

While coexisting model interferents (such as urea, creatinine, and common ions) remained within a stable ±5% baseline intensity threshold, application to a complex mango juice matrix yielded elevated spike recoveries between 107.5% and 114.0%. These elevated values indicate a noticeable matrix effect and partial positive interference from complex components endogenous to fruit juice. Ultimately, while this platform establishes a robust, stable, and cost-effective foundation for non-enzymatic glucose evaluation at millimolar levels, further surface engineering is required to mitigate complex food matrix interferences before routine adoption in industrial food quality monitoring.

REFERENCES

[1] Dey, K., Santra, T. S. & Tseng, F. G. (2025). Advancements in Glucose Monitoring: From Traditional Methods to Wearable Sensors, *Journal of Science Laboratory Technology*, 4(1), 1–31.

[2] Wang, J. (2008). Electrochemical Glucose Biosensors, Chemical Reviews, 108(2), 814–825.

[3] Shan, J., Li, J., Chu, X., Xu, M., Jin, F. & Wang, X. (2018). High-sensitivity glucose sensor built on MoS2-based field-effect transistors, RSC Advances, 8(3), 7942–7948.

[4] Xu, M., Nahar, L., Ritchie, K. J., Wang, C., Cheng, L., Wu, Z., Sarker, S. D. & Guo, M. (2025). Fluorescent platforms for bioactive carbohydrate evaluation, *Journal of Pharmaceutical Analysis*, 15(1), 101349.

[5] Zhang, Y., Cai, N. & Chan, V. (2023). Recent Advances in Silicon Quantum Dot-Based Fluorescent Biosensors, Biosensors, 13(3), 311–320.

[6] Morozova, S., Alikina, M., Vinogradov, A. & Pagliaro, M. (2020). Silicon Quantum Dots: Synthesis, Encapsulation, and Application in Light-Emitting Diodes, *Frontiers in Chemistry*, *8*(1), 1–8.

[7] Li, R., Xu, J., Mu, X. & Zeng, F. (2025a). A comprehensive review on the synthesis methods and applications of silicon quantum dots (SiQDs), *Next Nanotechnology*, 7(1), 100144.

[8] Zheng, S., Wang, H., Yu, Z., Chen, R., Yang, L., Xiong, B. & Tang, X. (2026). Nanoconfinement-Driven Solid-State Ratiometric Fluorescent Aptasensor for 17beta- Estradiol Detection in Complex Matrices, *Nigerian Journal of Chemical Sciences*, 14(2), 55– 63.

[9] The, B., Thangadurai, D. T., Sharipov, M., Ngoc, N., Cuong, N. Van & Lee, Y. (2022). Recent advances in turn off-on fluorescence sensing strategies for sensitive biochemical analysis - A mechanistic approach, *Microchemical Journal*, 179(2), 107511.

[10] Galant, A. L., Kaufman, R. C., & Wilson, J. D. (2015). Glucose: Detection and analysis, *Food Chemistry*, 188(1), 149–160.

[11] Huang, H., Li, H., Feng, J., Feng, H., Wang, A. & Qian, Z. (2017). One-pot green synthesis of highly fluorescent glutathione-stabilized copper nanoclusters for Fe3+ sensing, *Sensors & Actuators: B. Chemical*, 241(1), 292–297.

[12] Eda, H., Kara, S., Demirhan, B. & Demirhan, B. E. R. (2020). Highly luminescent water-dispersed silicon quantum dots for fluorometric determination of oxytetracycline in Milk samples, *Turkish Journal of Chemistry*, 44(6), 1713–1722.

[13] Li, Y., Li, W., Zhang, H., Liu, Y., Ma, L. & Lei, B. (2020). Amplified light harvesting for enhancing Italian lettuce photosynthesis using water soluble silicon quantum dots as artificial antennas, *Nanoscale*, 12(1), 155–166.

[14] Liu, Y., Zhang, X. & Wang, L. (2021). Fluorescence signatures of solution-processed silicon nanomaterials, *Journal of Luminescence*, 233(2), 117–124.

[15] Xu, M., Wang, X. & Chen, Y. (2019). Electronic state assignments in ultraviolet optical bands of group IV nanoparticles, Physical Chemistry Chemical Physics, 21(4), 1890–1898.

[16] Liu, J., Zhao, M., & Yang, B. (2022). Fine-tuning emission profiles of functionalized quantum dots for sensing, *Optics Express*, 30(2), 2415–2426.

[17] Beri, D., Busko, D., Mazilkin, A., Richards, B. S., Turshatov, A. & Howard, I. A. (2018). Surface oxidation parameters in green-prepared silicon core dots, RSC Advances, 8(2), 9979–9984.

[18] Shiohara, A., Hanada, S., Prabakar, S., Fujioka, K., Lim, T. H., Yamamoto, K., Northcote, P. T. & Tilley, R. D. (2010). Chemical Reactions on Surface Molecules Attached to Silicon Quantum Dots, *Langmuir*, 26(1), 248–253.

[19] Wang, Y., Wang, H., Guo, J., Wu, J., Gao, L. J., Sun, Y. H., Zhao, J. & Zou, G. F. (2015). Water-Soluble Silicon Quantum Dots with Quasi-Blue Emission, *Nanoscale Research Letters*, 10(1), 3–7.

[20] Abdelhameed, M., Martir, D. R., Chen, S., Xu, W. Z., Oyeneye, O. O., Chakrabarti, S., Zysman-Colman, E. & Charpentier, P. A. (2018). Tuning the Optical Properties of Silicon Quantum Dots via Surface Functionalization with Conjugated Aromatic Fluorophores, *Scientific Reports*, 8(1), 1–10.

[21] Anjiki, A. & Uchino, T. (2012). Visible Photoluminescence from Photoinduced Molecular Species in Nanometer-Sized Oxides, *Journal of Physical Chemistry C*, 116(4), 2315–2322.

[22] Terada, S., Xin, Y. & Saitow, K. (2020). Cost-Effective Synthesis of Silicon Quantum Dots, Chemistry of Materials, 32(14), 6010–6018.

[23] Elsayed, N. A., Aleppo, G., Aroda, V. R., Bannuru, R. R., Brown, F. M., Bruemmer, D. & Gabbay, R. A. (2023). Standards of Care in Diabetes—2023, *Diabetes Care*, 46(1), S68–S96.

[24] Holder, C. F. & Schaak, R. E. (2019). Tutorial on Powder X-ray Diffraction for Characterizing Nanoscale Materials, *ACS Nano*, 13(7), 7359–7365.

[25] Bukhtiyarova, M. V. (2019). A review on effect of synthesis conditions on the formation of layered double hydroxides, *Journal of Solid State Chemistry*, 269(1), 494–506.

[26] Talyzin, A. V., House, M. & Bond, G. (2019). Aggregation properties of solution-processed carbonaceous clusters, *Carbon*, 144(2), 312–320.

[27] Kim, H. & Lee, S. (2023). Concentration limits and optimization profiles of photoluminescent nanoparticle sensors, *Analytical Chemistry*, 95(4), 1812–1821.

[28] Vieira, N., Falaschi, C., Ryan, T. M., Primo, F. L., Greaves, T. L. & Pereira, J. F. B. (2020). Reversible and irreversible fluorescence activity of the Enhanced Green Fluorescent Protein in pH, *International Journal of Biological Macromolecules*, 164(1), 3474–3484.

[29] Li, R., Xu, J., Mu, X. & Zeng, F. (2025b). A comprehensive review on the synthesis methods and applications of silicon quantum dots (SiQDs), *Next Nanotechnology,* 7(2), 100144.

[30] Marunaka, Y. (2015). Roles of interstitial fluid pH in diabetes mellitus: Glycolysis and mitochondrial function, *World Journal of Diabetes*, 6(1), 125–135.

[31] Du, L., Li, Z., Yao, J., Wen, G., Dong, C. & Li, H. W. (2019). Enzyme free glucose sensing by amino-functionalized silicon quantum dot, Spectrochimica Acta - Part A: *Molecular and Biomolecular Spectroscopy*, 216(1), 303–309.